Supplementary materials for

Measurement report: The variation properties of aerosol hygroscopic growth related to chemical composition during new particle formation events in a coastal city of southeast China

Lingjun Li[1,2,3], Mengren Li[1,2,3*], Xiaolong Fan[1,2,3], Yuping Chen[1,2,3], Ziyi Lin[1,2,3], Anqi Hou[1,2], Siqing Zhang[1,2,3], Ronghua Zheng[1,2,3], Jinsheng Chen[1,2,3*]

[1] CAS Center for Excellence in Regional Atomospheric Environment, Institude of Urban Environment, Chinese Academy of Sciences, Xiamen 361021, China;

[2] Fujian Key Laboratory of Atmospheric Ozone Pollution Prevention, Institute of Urban Environment, Chinese Academy of Sciences, Xiamen 361021, China;

[3] College of Resources and Environment, University of Chinese Academy of Sciences, Beijing 100086, China

* Corresponding to: Jinsheng Chen (jschen@iue.ac.cn) and Mengren Li (mrli@iue.ac.cn)

Table S1. The hygroscopicity parameters (κ) and densities (ρ) of inorganic salts used in this study.

Species	NH_4NO_3	$(NH_4)_2SO_4$	NH_4HSO_4	NH_4Cl
κ	0.58	0.48	0.56	0.93
ρ (g cm^{-3})	1.72	1.769	1.78	1.527

Table S2. Comparisons of the average *f*(80%) or *f*(85%) values in different study.

Study area	Periods	*f*(RH)	RH(%)	Reference
Lin'an, China	2013/3/1-31	1.43 ± 0.12	80	Zhang et al. (2015)
		1.58 ± 0.12	85	
Raoyang, China	2014/6/17 - 8/16	2.28 ± 0.69	80	Wu et al. (2017)
		3.39 ± 1.14	85	
Beijing, China	2017/1/12 – 2/14	1.47 ± 0.16	80	Zhao et al. (2019)
Beijing, China	2019/9/19 - 10/4	1.64 ± 0.13	85	Ren et al. (2021)
Guangzhou, China	2019/10/15 - 2020/1/8	1.50 ± 0.11	70	Li et al. (2021)
Ny- Ålesund, Svalbard	2008/7/15 – 10/13	3.24 ± 0.63	85	Zieger et al. (2010)
Jungfraujoch, Swiss	2008/5	2.30 ± 0.33	85	Zieger et al. (2013)
Mace Head, Ireland	2009/1-2	2.08 ± 0.29	85	
Granada, Spain	2013/4/4 – 5/10	1.60 ± 0.30	85	Titos et al. (2014)
Xiamen, China	2022/2 - 4	1.44 ± 0.15	80	This study
		1.60 ± 0.16	85	

Table S3. Statistical analysis of particle concentration distribution (cm^{-3}) for different days from February to April 2022.

		NPF	Undefined	Non-NPF	Entire campaign
Total	mean	6.31×10^{3}	5.72×10^{3}	3.41×10^{3}	5.29×10^{3}
	stdv	3.60×10^{3}	2.61×10^{3}	1.91×10^{3}	2.82×10^{3}
	max	1.67×10^{4}	3.05×10^{4}	1.15×10^{4}	3.05×10^{4}
	median	5.60×10^{3}	5.37×10^{3}	2.82×10^{3}	4.91×10^{3}
	min	1.08×10^{3}	6.57×10^{2}	5.50×10^{2}	5.50×10^{2}
Nucleation mode	mean	1.66×10^{3}	1.15×10^{3}	6.99×10^{2}	1.12×10^{3}
	stdv	1.59×10^{3}	8.25×10^{2}	5.16×10^{2}	9.52×10^{2}
	max	8.34×10^{3}	8.57×10^{3}	5.28×10^{3}	8.57×10^{3}
	median	1.06×10^{3}	9.40×10^{2}	5.81×10^{2}	8.64×10^{2}
	min	1.05×10^{2}	6.59×10	2.00×10	2.00×10
Aitken mode	mean	3.80×10^{3}	3.37×10^{3}	1.78×10^{3}	3.08×10^{3}
	stdv	2.80×10^{3}	1.82×10^{3}	1.08×10^{3}	1.98×10^{3}
	max	1.44×10^{4}	2.21×10^{4}	6.09×10^{3}	2.21×10^{4}
	median	2.97×10^{3}	3.10×10^{3}	1.43×10^{3}	2.73×10^{3}
	min	5.47×10^{2}	3.02×10^{2}	2.60×10^{2}	2.60×10^{2}
Accumulation mode	mean	8.59×10^{2}	1.20×10^{3}	9.33×10^{2}	1.10×10^{3}
	stdv	4.04×10^{2}	6.12×10^{2}	6.20×10^{2}	6.0810^{2}
	max	2.42×10^{3}	7.67×10^{3}	4.99×10^{3}	7.67×10^{3}
	median	7.82×10^{2}	1.11×10^{3}	7.55×10^{2}	1.01×10^{3}
	min	2.09×10^{2}	3.73×10	8.75×10	3.73×10

Table S4. The curve-fitting parameters for *f*(RH) for different aerosol types using Eq.(1).

		a	*b*	Reference
Entire campaign	RH < 60%	1.02	0.21	Chen et al. (2014)
	RH ≥ 60%	1.08	0.26	
Clean	RH < 60%	1.00	0.10	
	RH ≥ 60%	1.00	0.26	
Polluted	RH < 60%	1.03	0.26	
	RH ≥ 60%	1.14	0.25	
Very clean	12 Jan.-14 Feb. 2017	0.930	0.329	Zhao et al. (2019)
Moderately clean		0.971	0.372	
Polluted		0.988	0.356	
Very clean	6 July-21 Aug. 2017	0.972	0.355	
Moderately clean		0.980	0.362	
Polluted		0.984	0.371	
Very clean	30 Sep.-13 Nov. 2017	0.979	0.334	
Moderately clean		1.002	0.344	
Polluted		1.014	0.332	
NPF	Feb.-Apr. 2022	0.993	0.257	This work
Non-NPF		1.026	0.289	

Table S5. Statistics on the mass concentration (μg m^{-3}) of aerosol species (S.D.: standard deviation)

	Mean	S.D.	Maximum	Minimum
Sulfate	1.82	1.08	6.54	0.02
Nitrate	2.75	3.28	24.46	0.03
Ammonium	1.26	1.04	6.26	0.02
Chlorine	0.16	0.17	1.89	0.001
OM	4.84	3.85	52.22	0.18
BC	0.95	0.62	3.51	0.10

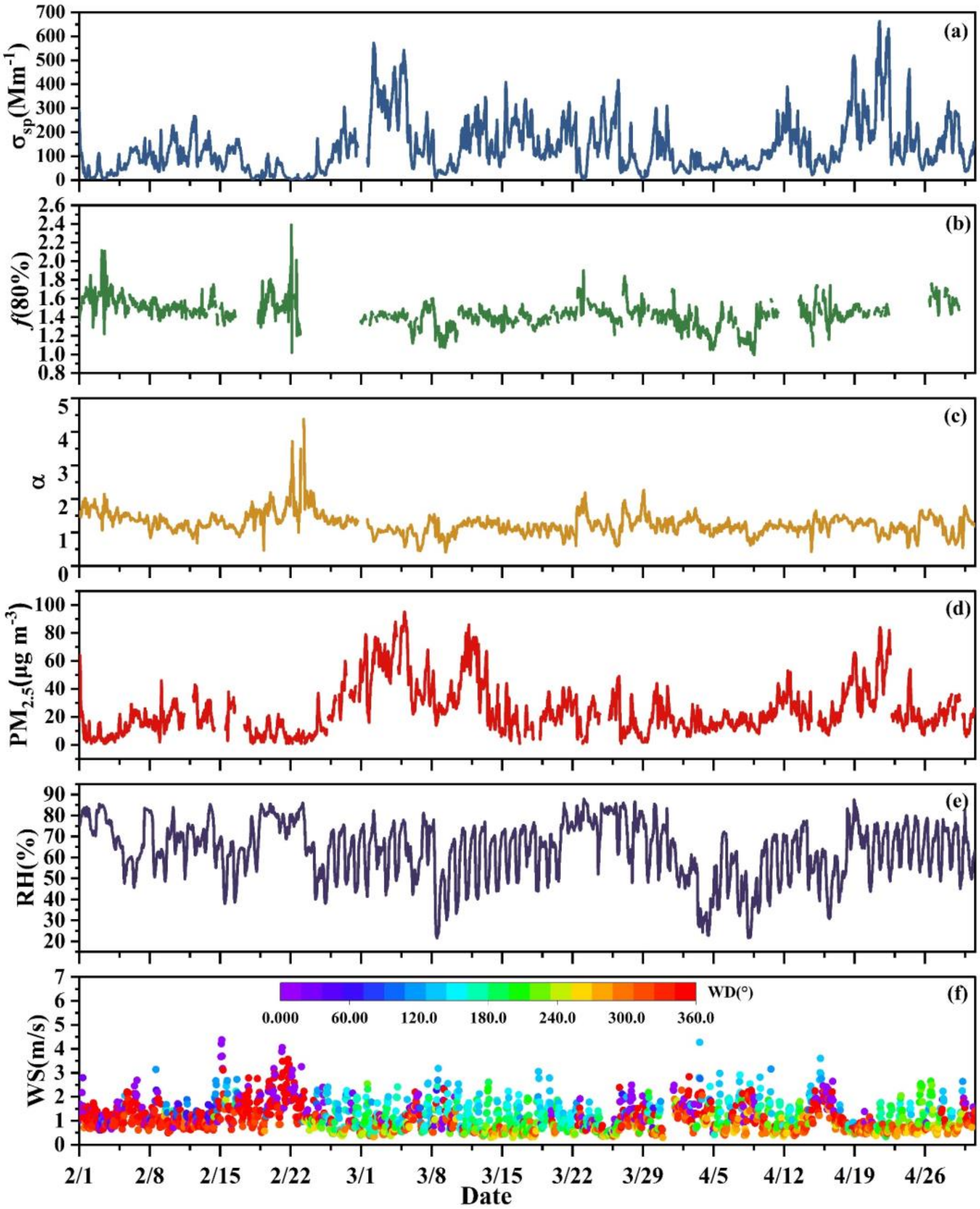

Figure S1. Time series of measured and derived aerosol variables and ambient RH, wind speed and direction from February to April 2022. (a) Aerosol scattering coefficient of DryNeph at 525 nm wavelength; (b) the aerosol scattering hygroscopic growth factor *f*(80%) at 525 nm wavelength; (c) scattering Ångström exponents α; (d) $PM_{2.5}$ mass concentrations; (e) relative humidity (RH) at ambient conditions; (f) wind speeed (WS) and wind direction (WD).

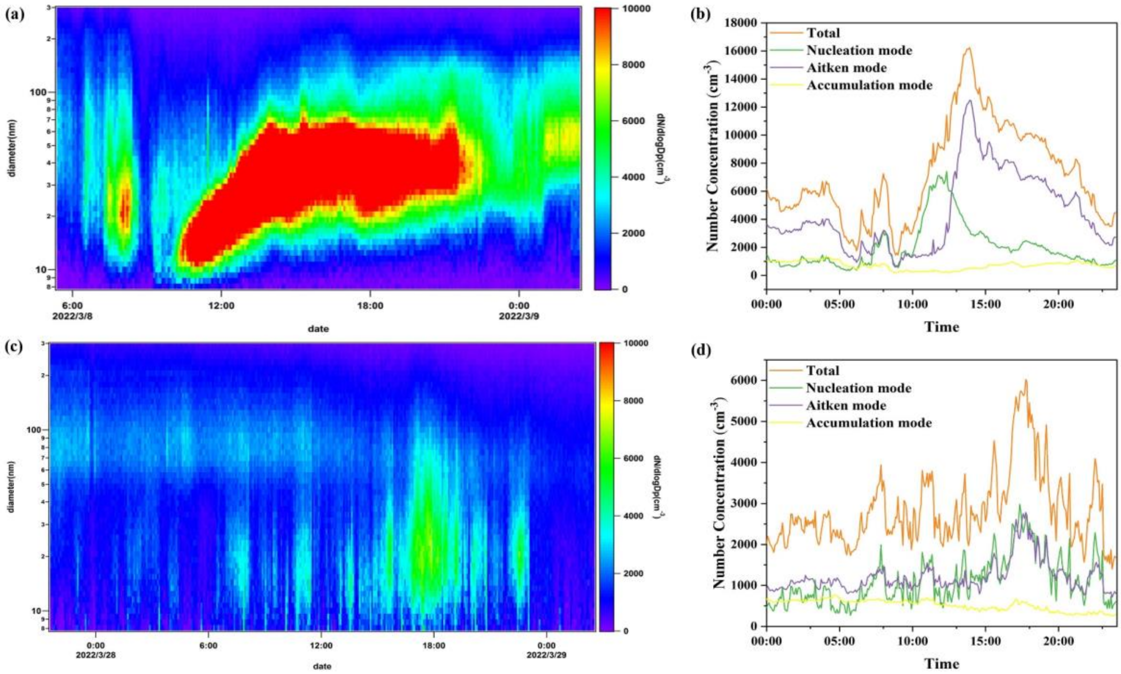

Figure S2. the particle number size distribution spectrum and number concentration. Example of NPF (a, b) and Non-NPF (c, d) days.

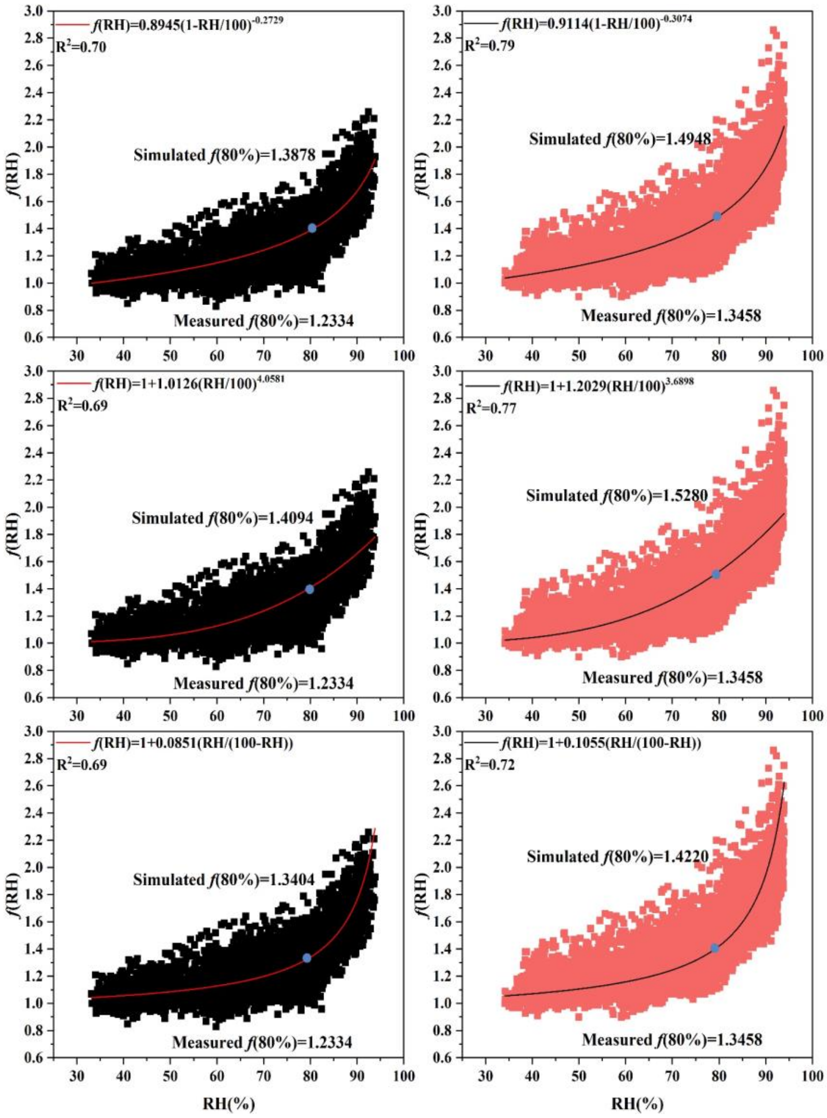

Figure S3. Comparisons of the *f*(RH) fitted curves following the other three parameterization schemes between NPF and Non-NPF events. Black: NPF, red: Non-NPF. The first column shows the results fitted by Eq. (S4), the second column shows the results fitted by Eq. (S5), and the third column shows the results fitted by Eq. (S6).

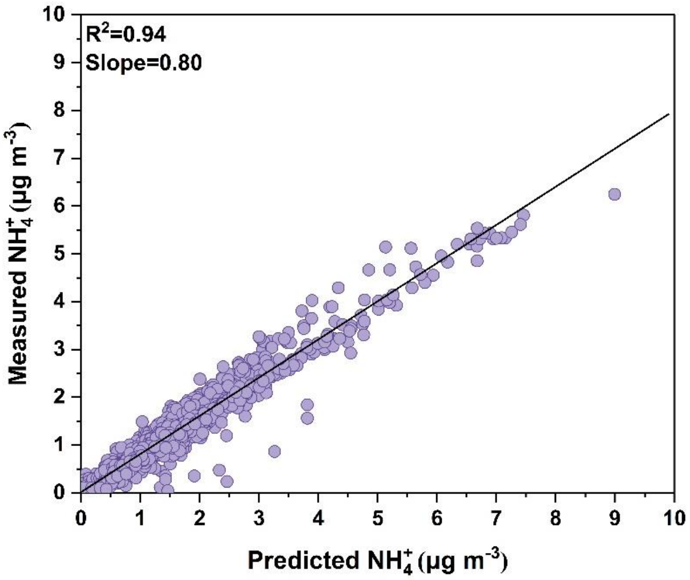

Figure S4. Measured and predicted mass concentration of ammonium. The predicted mass concentration of ammonium (predicted NH_4^+) is calculated by Eq. (S5). The solid line represents the linear regression.

Text S1.

The κ_{chem} of this study can be calculated by the following equation(Petters and Kreidenweis, 2007):

$$\kappa_{chem} = \sum_i \kappa_i \cdot \varepsilon_i \quad \text{(S1)}$$

where κ_i and ε_i denote the hygroscopicity parameter κ and the volume fraction of chemical component i in the aerosol. Based on Eq.(S6) and Supplementary Table S5, κ_{chem} can be expressed as follows:

$$\kappa_{chem} = \kappa_{AN}\varepsilon_{AN} + \kappa_{AS}\varepsilon_{AS} + \kappa_{ABS}\varepsilon_{ABS} + \kappa_{AC}\varepsilon_{AC} + \kappa_{BC}\varepsilon_{BC} + \kappa_{OA}\varepsilon_{OA} \quad \text{(S2)}$$

Where, κ_{BC} is the κ of the black carbon aerosol (BC), which is assumed to be zero because BC is hydrophobic; κ_{OA} and ε_{OA} represent the κ and volume fraction of the total organic matter. The total aerosol volume concentration used to calculate the volume fraction was calculated by summing the volume concentrations of all chemical species (AN, AS, ABS, AC, BC and OA), where the volume concentration of BC was calculated by assuming a density of 1.7 g cm^{-3} (Wu et al., 2016).

Text S2.

There are some characteristics of NPF and Non-NPF events (Figure S2). When NPF events occurred, the particle number size distribution showed an obvious "banana shape", and the nucleation-mode particles exhibited a clear growth process for several hours. In Non-NPF days, the concentration of nucleation-mode particles did not exhibit a notable peak, and the growth process of particles did not appear. The onset time of NPF events observed in this study typically occurred around 10:00, coinciding with a sudden and rapid increase in the number concentration of nucleation-mode particles (N_{nuc}). The diurnal variation of N_{nuc} exhibited a unimodal pattern, with the peak concentration occurring around 12:00. Following the increase in N_{nuc}, the number concentration of aitken-mode particles subsequently rose, reaching a peak concentration around 15:00, with a time delay of several hours after the peak of nucleation-mode particles, mainly caused by growth progress of particles from nucleation mode to a larger particle size range.

Text S3.

The f(RH) values were fitted with four frequently-used empirical equations. The comparison of the fitting results, R^2 values, simulated and measured values of f(80%) for each parameterization scheme reveals that Eq. (S1) had the best fitting curve, the highest R^2 value, and it also had the smallest difference between simulated and measured values of f(80%). Therefore, Eq. (S1) was considered to be the most suitable parameterization scheme.The fitted curves of the other three parameterization schemes are shown in Figure S3.

$$f(\mathrm{RH}) = a(1-\frac{RH}{100})^{-b(\frac{\mathrm{RH}}{100})} \quad \text{(S3)(Chen et al., 2014)}$$

$$f(\mathrm{RH}) = a(1-\frac{\mathrm{RH}}{100})^{-b} \quad \text{(S4)(Kasten, 1969)}$$

$$f(\mathrm{RH}) = 1 + a(\frac{\mathrm{RH}}{100})^{b} \quad \text{(S5)(Kotchenruther and Hobbs, 1998)}$$

$$f(\mathrm{RH}) = 1 + a(\frac{\mathrm{RH}}{100-\mathrm{RH}}) \quad \text{(S6)(Brock et al., 2016)}$$

Text S4.

Aerosol acidity is a crucial parameter affecting the aerosol hygroscopic growth. This is usually assessed by comparing the measured mass concentration of NH_4^+ with the amount required to completely neutralize sulfate, nitrate, and chloride ions (predicted NH_4^+), which can be obtained from the following equation (Sun et al., 2010):

$$\text{predicted } \mathrm{NH_4^+} = 18 \times (2 \times \frac{SO_4^{2-}}{96} + \frac{NO_3^-}{62} + \frac{Cl^-}{35.5}) \quad \text{(S7)}$$

The relationship between measured NH_4^+ and predicted NH_4^+ was demonstrated by Figure S4. The correlation between measured and predicted NH_4^+ was very strong (r^2=0.94), with a regression slope of 0.8, revealing that there were insufficient atmospheric NH_4^+ to fully neutralise sulfate and nitrate, thereby, PM_1 in Xiamen was considered to be more acidic during the observation period. Thus, the main chemical form of the sulfate aerosol was NH_4HSO_4, and the nitrate aerosol was in the form of NH_4NO_3. However, the average mass concentration of chloride ions was low in Xiamen during observation period, so the mass concentration of NH_4Cl was also low, with NH_4NO_3, NH_4HSO_4 and $(NH_4)_2SO_4$ as the dominant inorganic components.

Supplementary References

Brock, C. A., Wagner, N. L., Anderson, B. E., Attwood, A. R., Beyersdorf, A., Campuzano-Jost, P., Carlton, A. G., Day, D. A., Diskin, G. S., Gordon, T. D., Jimenez, J. L., Lack, D. A., Liao, J., Markovic, M. Z., Middlebrook, A. M., Ng, N. L., Perring, A. E., Richardson, M. S., Schwarz, J. P., Washenfelder, R. A., Welti, A., Xu, L., Ziemba, L. D., and Murphy, D. M.: Aerosol optical properties in the southeastern United States in summer - Part 1: Hygroscopic growth, Atmospheric Chemistry and Physics, 16, 4987-5007, 10.5194/acp-16-4987-2016, 2016.

Chen, J., Zhao, C. S., Ma, N., and Yan, P.: Aerosol hygroscopicity parameter derived from the light scattering enhancement factor measurements in the North China Plain, Atmospheric Chemistry and Physics, 14, 8105-8118, 10.5194/acp-14-8105-2014, 2014.

Kasten, F.: VISIBILITY FORECAST IN PHASE OF PRE-CONDENSATION, Tellus, 21, 630-&, 10.1111/j.2153-3490.1969.tb00469.x, 1969.

Kotchenruther, R. A., and Hobbs, P. V.: Humidification factors of aerosols from biomass burning in Brazil, Journal of Geophysical Research-Atmospheres, 103, 32081-32089, 10.1029/98jd00340, 1998.

Li, J. W., Zhang, Z. S., Wu, Y. F., Tao, J., Xia, Y. J., Wang, C. Y., and Zhang, R. J.: Effects of chemical compositions in fine particles and their identified sources on hygroscopic growth factor during dry season in urban Guangzhou of South China, Science of the Total Environment, 801, 10.1016/j.scitotenv.2021.149749, 2021.

Petters, M. D., and Kreidenweis, S. M.: A single parameter representation of hygroscopic growth and cloud condensation nucleus activity, Atmospheric Chemistry and Physics, 7, 1961-1971, 10.5194/acp-7-1961-2007, 2007.

Ren, R. M., Li, Z. Q., Yan, P., Wang, Y. Y., Wu, H., Cribb, M., Wang, W., Jin, X. A., Li, Y. A., and Zhang, D. M.: Measurement report: The effect of aerosol chemical composition on light scattering due to the hygroscopic swelling effect, Atmospheric Chemistry and Physics, 21, 9977-9994, 10.5194/acp-21-9977-2021, 2021.

Sun, J. Y., Zhang, Q., Canagaratna, M. R., Zhang, Y. M., Ng, N. L., Sun, Y. L., Jayne, J. T., Zhang, X. C., Zhang, X. Y., and Worsnop, D. R.: Highly time- and size-resolved characterization of submicron aerosol particles in Beijing using an Aerodyne Aerosol Mass Spectrometer, Atmospheric Environment, 44, 131-140, 10.1016/j.atmosenv.2009.03.020, 2010.

Titos, G., Lyamani, H., Cazorla, A., Sorribas, M., Foyo-Moreno, I., Wiedensohler, A., and Alados-Arboledas, L.: Study of the relative humidity dependence of aerosol light-scattering in southern Spain, Tellus Series B-Chemical and Physical Meteorology, 66, 10.3402/tellusb.v66.24536, 2014.

Wu, Y. F., Wang, X. J., Yan, P., Zhang, L. M., Tao, J., Liu, X. Y., Tian, P., Han, Z. W., and Zhang, R. J.: Investigation of hygroscopic growth effect on aerosol scattering coefficient at a rural site in the southern North China Plain, Science of the Total Environment, 599, 76-84, 10.1016/j.scitotenv.2017.04.194, 2017.

Wu, Z. J., Zheng, J., Shang, D. J., Du, Z. F., Wu, Y. S., Zeng, L. M., Wiedensohler, A., and Hu, M.: Particle hygroscopicity and its link to chemical composition in the urban atmosphere of Beijing, China, during summertime, Atmospheric Chemistry and Physics, 16, 1123-1138, 10.5194/acp-16-1123-2016, 2016.

Zhang, L., Sun, J. Y., Shen, X. J., Zhang, Y. M., Che, H., Ma, Q. L., Zhang, Y. W., Zhang, X. Y., and Ogren, J. A.: Observations of relative humidity effects on aerosol light scattering in the Yangtze River Delta of China, Atmospheric Chemistry and Physics, 15, 8439-8454, 10.5194/acp-15-8439-2015, 2015.

Zhao, P. S., Ding, J., Du, X., and Su, J.: High time-resolution measurement of light scattering hygroscopic growth factor in Beijing: A novel method for high relative humidity conditions, Atmospheric Environment, 215, 10.1016/j.atmosenv.2019.116912, 2019.

Zieger, P., Fierz-Schmidhauser, R., Gysel, M., Strom, J., Henne, S., Yttri, K. E., Baltensperger, U., and Weingartner, E.: Effects of relative humidity on aerosol light scattering in the Arctic, Atmospheric Chemistry and Physics, 10, 3875-3890, 10.5194/acp-10-3875-2010, 2010.

Zieger, P., Fierz-Schmidhauser, R., Weingartner, E., and Baltensperger, U.: Effects of relative humidity on aerosol light scattering: results from different European sites, Atmospheric Chemistry and Physics, 13, 10609-10631, 10.5194/acp-13-10609-2013, 2013.